

## Article

# Comparison of the Mechanical Properties and Corrosion Resistance of the Cr-CrN, Ti-TiN, Zr-ZrN, and Mo-MoN Coatings

He Tao <sup>1</sup>, Valery Zhylinski <sup>2,\*</sup>, Alexey Vereschaka <sup>3</sup>, Vadzim Chayauski <sup>4</sup>, Huo Yuanming <sup>1,\*</sup>,  
Filipp Milovich <sup>5</sup>, Catherine Sotova <sup>6</sup>, Anton Seleznev <sup>6</sup> and Olga Salychits <sup>2</sup>

- <sup>1</sup> School of Mechanical and Automotive Engineering, Shanghai University of Engineering Science, No. 333 Longteng Road, Shanghai 201620, China; hetao@sues.edu.cn
- <sup>2</sup> Department of Chemistry, Technology of Electrochemical Production and Electronic Engineering Materials, Chemical Technology and Engineering Faculty, Belarusian State Technological University, 13a, Sverdlov Street, 220006 Minsk, Belarus; olisa\_@list.ru
- <sup>3</sup> Institute of Design and Technological Informatics of the Russian Academy of Sciences (IDTI RAS), Vadkovsky per. 18-1a, 127994 Moscow, Russia; dr.a.veres@yandex.ru
- <sup>4</sup> Department of Physics, Faculty of Information Technology, Belarusian State Technological University, 13a, Sverdlov Street, 220006 Minsk, Belarus; doctorv\_v\_ch@mail.ru
- <sup>5</sup> Materials Science and Metallurgy Shared Use Research and Development Center, National University of Science and Technology MISiS, Leninsky Prospect 4, 119049 Moscow, Russia
- <sup>6</sup> Department of High-Efficiency Machining Technologies, Moscow State Technological University STANKIN, Vadkovsky per. 1, 127994 Moscow, Russia; e.sotova@stankin.ru (C.S.)
- \* Correspondence: zhilinski@yandex.ru (V.Z.); yuanming.huo@sues.edu.cn (H.Y.)

**Abstract:** In this work, the mechanical properties and corrosion resistance of Cr-CrN, Ti-TiN, Zr-ZrN, and Mo-MoN coatings deposited by the physical vapor deposition (PVD) method on Ti-6Al-4V alloy were compared. The phase composition of the coatings, their hardness and fracture resistance in scratch tests were determined, and their structural characteristics were also studied using a scanning electron microscope (SEM) and a transmission electron microscope (TEM). The diffraction spectra were made using an automatic X-ray diffractometer. The value of the adhesive component of the friction coefficient  $f_{adh}$  of the pair “coated and uncoated Ti-6Al-4V alloy” was investigated in the temperature range of 20–900 °C. The lowest value of  $f_{adh}$  was detected for the Zr-ZrN coating at temperatures below 400 °C, while for the Mo-MoN coating it was observed at temperatures above 700 °C. The polarization curves of the coated and uncoated samples were performed in a 3% aqueous NaCl solution. The level of corrosion of the Ti-6Al-4V alloy samples with Cr-CrN, Ti-TiN, Zr-ZrN, and Mo-MoN coatings was evaluated using the Tafel extrapolation method, the iteration method, and the polarization resistance method. The results obtained with these methods indicate that the Zr-ZrN coated sample has the best corrosion resistance in the 3 wt.% NaCl solution, with a corrosion current density of 0.123  $\mu\text{A}/\text{cm}^2$ .

**Keywords:** nitride coatings; corrosion; polarization curves; titanium alloy; tribological properties



**Citation:** Tao, H.; Zhylinski, V.; Vereschaka, A.; Chayauski, V.; Yuanming, H.; Milovich, F.; Sotova, C.; Seleznev, A.; Salychits, O. Comparison of the Mechanical Properties and Corrosion Resistance of the Cr-CrN, Ti-TiN, Zr-ZrN, and Mo-MoN Coatings. *Coatings* **2023**, *13*, 750. <https://doi.org/10.3390/coatings13040750>

Academic Editor: Luigi Calabrese

Received: 18 March 2023

Revised: 3 April 2023

Accepted: 6 April 2023

Published: 8 April 2023



**Copyright:** © 2023 by the authors. Licensee MDPI, Basel, Switzerland. This article is an open access article distributed under the terms and conditions of the Creative Commons Attribution (CC BY) license (<https://creativecommons.org/licenses/by/4.0/>).

## 1. Introduction

Titanium alloys are widely used as structural materials in a variety of industries, including aircraft and rocket construction, medical products, engine construction, and several other areas of mechanical engineering [1–7]. Although titanium is a highly active metal, a dense oxide film formed on its surface prevents further oxidation and interaction with aggressive media [8–12]. However, this film can be damaged by several factors, including electrolytic processes, chemical, mechanical, and thermal effects, etc., which can lead to active corrosion of titanium products. This interaction with the environment can have negative effects on both the titanium products themselves and the media that

interact with them (e.g., titanium-induced metallosis of Ti-6Al-4V and Ti-Ni alloys in medicine) [13–15]. The physical vapor deposition (PVD) method of modifying the surface properties of products by depositing special coatings on their surfaces is widely used to solve various problems, including increasing hardness, wear resistance, modifying tribological properties, and reducing adhesive and diffusive interactions [16,17]. The PVD coatings on product surfaces to improve their corrosion resistance are also widely used in various industrial sectors such as aircraft, rocket and engine construction, medical products, and mechanical tools [18,19].

Although PVD coating multi-component and multi-layer systems are often considered anticorrosive coatings, two-component nitrides of TiN, CrN, ZrN, and MoN are still widely used in biomedical implants based on Ti alloys [20]. These systems will be examined and compared on their anticorrosive properties for the Ti alloys in aggressive media.

The TiN coating is one of the first PVD-deposited nitride coatings. This coating is still actively used in various fields, including increasing the corrosion resistance of products made from titanium alloys and steels of various compositions [21–30]. It had been reported in the literature that the TiN coatings did not provide complete corrosion protection [21,31,32] and that they only experienced slight corrosion along the grain boundaries of the TiN coatings when they were exposed at a temperature of 500 °C onto the NaCl crystals [31]. The interaction between TiN and NaCl results in the formation of TiO<sub>2</sub> and a small amount of Na<sub>x</sub>Ti<sub>y</sub>O<sub>z</sub>. It is the defects in the TiN coating, including cracks, pores, etc., that are the main cause of corrosion [31,32]. Various authors have shown that an intermediate layer between the substrate and the Ti coating can increase its corrosion resistance [33–35]. This Ti-based interlayer also has a positive effect on the corrosion resistance of the Ti-(Ti,Al)N coating deposited on titanium alloys in a solution of NaCl, H<sub>2</sub>O, and O<sub>2</sub> at a temperature of 600 °C [36]. The corrosion resistance of the TiN coating can be improved by an additional heat treatment in air at a temperature of 800 °C [32]. This improvement was associated with a decrease in coating defects, which in turn can be explained by the formation of TiO<sub>2</sub> and Ti<sub>2</sub>O<sub>3</sub> oxides in the TiN structure due to volumetric expansion that has taken place and a coating microstructure that has become more dense. The thickness of the coating also affects the corrosion resistance; and, in theory, a thicker coating provides the best corrosion resistance, but studies show that a coating that is too thick has a lower corrosion resistance. The increasing thickness of the Ti-TiN coating leads to an increase in the number of internal defects in the coating, through which oxygen actively diffuses into the deeper layers in violation of the coating structure, e.g., around embedded microparticles, and the columnar grain boundary, which increases with increasing coating thickness [37]. Oxidation of the inner layers of the coating leads to expansion of their volume, increased internal stresses, and active cracking, which cause their failure [37].

In addition to TiN coatings, other two-component nitride coatings are also used for corrosion protection, such as CrN [35,38–48], ZrN [49–51], and MoN [52,53].

Tests reveal the high anticorrosive properties of CrN coatings in multi-component physiological solutions, such as Ringer's and Hank's solutions [44]. CrN-coated samples have half the corrosion potential and ten times the corrosion current density of uncoated samples. The CrN coating resists oxidation well at high temperatures up to 1160 °C [45]. The corrosion resistance of the CrN coating increases with the density of its microstructure and the decrease in the level of residual stresses [46]. The thickness of the coating also affects its corrosion resistance. The CrN coating with a thickness of 3 to 4 μm provides a 10-fold reduction in corrosion current density ( $i_{\text{corr}}$ ) compared to the uncoated aluminum alloy sample, while a 5 μm thick coating provides a 20-fold reduction [38]. In contrast to the columnar structure of TiN, the non-column structure of the CrN crystallite has a lower open porosity [47,48]. Diffusion of reagents in the CrN coating occurs in a zigzag pattern, due to which the diffusion process can be slowed down [48].

The Cr interlayer in the Cr-CrN coating, as well as the Ti layer in the Ti-TiN coating, improve the corrosion resistance of the corresponding coatings [49]. Furthermore, the use

of a pure metal interlayer significantly increases the adhesion between the coating and the substrate and increases the corrosion resistance [50].

The ZrN coating has also been shown to have interesting anti-corrosion properties [51–53]. By increasing the temperature, it has been shown that the effect of the atmosphere on the ZrN coating leads to the formation of  $ZrN_xO_y$  and  $ZrO_2$  on its surface, which further increases its pitting resistance [51]. It has also been shown that the ZrN coating significantly increases the corrosion resistance in an aqueous  $Na_2SO_4$  solution [52], as well as the charge transfer resistance, which increases by 122 times [53]. This decrease in the degradative intensity of the corrosion process was attributed to the high density and strong adhesion of the ZrN coating, which prevents electrolyte penetration, reduces contact areas between the alloy and the corrosive agent, modifies the charge transfer process in electrochemical reactions, and prevents delamination of the coating [53].

The MoN coating has been considered an anticorrosion coating much less often [54,55]. In particular, the MoN coating was found to have a lower tendency to crack but a higher susceptibility to degradation under the influence of  $H_3PO_4$  and  $H_2SO_4$  solutions compared to the TiN coating [55].

Comparison of the properties of CrN and TiN coatings reveals that the CrN coating offers better corrosion protection than the TiN coating [56,57]. Comparison of the corrosion resistance of Ti-TiN, Cr-TiN, and Cr-CrN coatings shows that the Cr-CrN coating has clear advantages and high corrosion resistance for all the coatings compared [58]. The CrN coating showed better oxidation resistance than TiN coatings in 3.5 wt.% NaCl solution and in 1 M  $H_2SO_4$  solution [59,60]. Comparison of the corrosion currents of TiN ( $0.099 \mu A/cm^2$ ) and ZrN ( $0.209 \mu A/cm^2$ ) coatings with a thickness of 3  $\mu m$  showed that the TiN coating has better corrosion resistance than the ZrN coating [61]. Meanwhile, the comparison of the corrosion resistance of TiN, CrN, and ZrN coatings in anion-based ionic liquids reveals that the ZrN coating has the highest corrosion resistance [62]. There are many studies on the corrosion resistance of coatings containing layers of various two-component nitrides; for example, ZrN-CrN coatings have shown extremely high corrosion resistance in NaCl solution [63].

The (Ti,Mo)N coating has the lowest corrosion resistance compared to the reference TiN coating, and the corrosion resistance of the coating decreases as the Mo content increases [64]. At the same time, the introduction of Mo into the CrN coating improves its corrosion resistance compared to the uncoated sample and the sample with the CrN coating containing no molybdenum [65]. Good corrosion protection was provided by the (Mo,Ti)N coating [55].

The analysis of the studies [21–65] considered suggests the following ranking of nitrides coatings from the worst to the best corrosion resistance:

$$CrN < TiN < ZrN < MoN.$$

The authors are not aware of any articles comparing the corrosion properties of the four nitride coatings on Ti alloys under the same experimental conditions. Furthermore, some reported results do not agree with the sequence presented above (e.g., ZrN has the best properties in terms of corrosion resistance [62]), whereas the corrosion resistance of Cr-CrN, Ti-TiN, Zr-ZrN, and Mo-MoN coatings is the most important parameter that determines the areas in which they can be applied.

The objective of this investigation was therefore to carry out a comprehensive study of the tribological characteristics of ion-plasma-prepared coatings based on Cr-CrN, Ti-TiN, Zr-ZrN, and Mo-MoN on Ti-6Al-4V alloy and their corrosion properties in 3% aqueous NaCl solution using the polarization curve method. The studied nitride coatings are quite often considered as corrosion protection; however, a comprehensive comparison of their properties has not been previously carried out in full, and such a comparison may be useful for substantiating the choice of coatings and further studies of coatings of a more complex composition.

## 2. Materials and Methods

The investigations were carried out on Cr-CrN, Ti-TiN, Zr-ZrN, and Mo-MoN coatings deposited on Ti-6Al-4V titanium alloy plates (Figure 1a). Titanium plates were made on a lathe, and thus their surfaces (both end and side) were formed as a result of turning. Sample sizes are shown in Figure 1a.

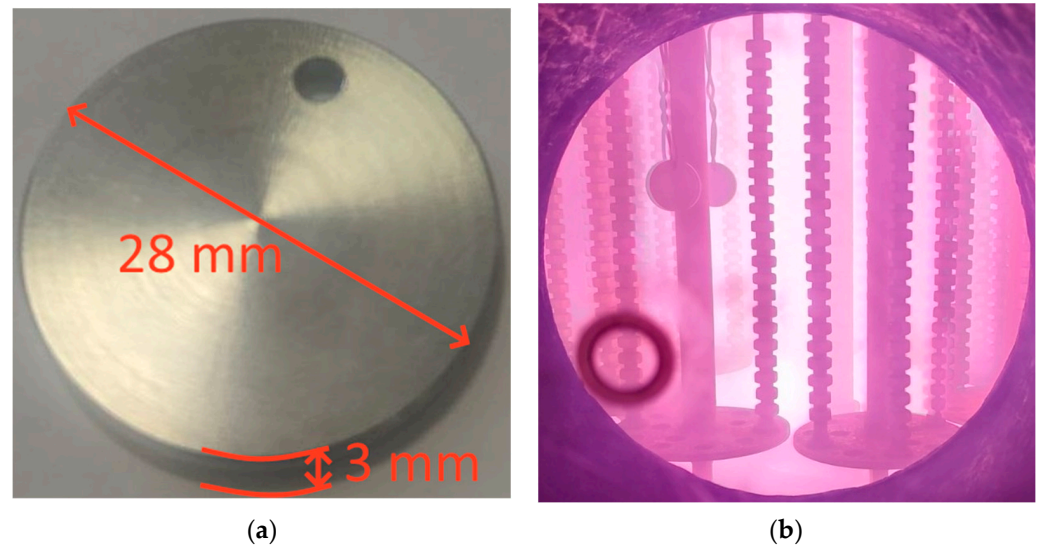


**Figure 1.** Optical microscopy image showing the dimensions of the sample (a) and the coating process (b).

The chemical composition of Ti-6Al-4V alloy is described in Table 1.

**Table 1.** Chemical composition of Ti-6Al-4V alloy identified by EDX analysis.

Elements	Fe	C	Si	V	Ti	Al	Zr	Others
Partition, wt. %	~0.6	~0.1	~0.1	3.5–5.3	86.5–90.9	5.3–6.8	~0.3	~0.6

The coatings were deposited using an upgraded VIT-2 vacuum plasma unit [66–70], (IDTI RAS-MSTU STANKIN, Moscow, Russia). This unit uses a combination of filtered vacuum cathode deposition (FCVD) [71–76] and controlled accelerated arc deposition (CAA-PVD) technologies [77,78]. Cathodes of Cr (99.9%), Mo (99.8%), Zr (99.8%), and Ti (99.6%) were used. The placement of the samples during the coating process is shown in Figure 1b. Before coating deposition, the samples were subjected to washing in a special solution with ultrasonic stimulation. During the deposition process, the samples were subjected to preliminary ion cleaning in order to thermally activate the surface and remove residual contaminants and oxide films.

The main parameters of the coating deposition process are presented in Table 2.

**Table 2.** Main parameters of the coating deposition process at pressure  $N_2$  0.42 Pa and voltage of substrate  $-150$  V (DC).

Cathode	Ti	Zr	Cr	Mo
Arc current (A)	75	65	78	80

The special technique and equipment developed in co-operation with USATU-IDTI RAS-MSTU STANKIN [79–82] were used to study the tribological properties of the samples. When the samples were tested under conditions simulating real friction pair contact, the strength of adhesive bonds  $\tau_{nm}$  and the value of normal stresses  $P_{nm}$  were determined. The

specimen consists of a Ti-6Al-4V alloy bar, with and without the studied coating, which is clamped between two parallel Ti-6Al-4V alloy plates (the setup diagram is described in more detail in [79–82]). The plates press an indenter with varying forces, and at the same time, the contact area between the indenter and the plates is heated from 20 to 900 °C. Tribological parameters were determined at temperatures of 20, 400, 700, 800, and 900 °C. In addition, the contact conditions were simulated at constant loads and at different temperatures. The force  $F_{exp}$  was measured directly by rotating the indenter located between two flat plates and pressing it with the force  $F_{sq}$ . The values of  $\tau_{nn}$  and  $P_{rn}$  were calculated based on the magnitude of the  $F_{exp}$  force [79–82]. The adhesive component of the friction coefficient  $f_{adh}$  was calculated using the following formula:

$$f_{adh} = \frac{\tau_{nn}}{P_{rn}} \quad (1)$$

The diffraction spectra were made using an automatic X-ray diffractometer, DRON-4 (LNPO Burevestnik, S-Petersburg, Russia), using monochromatic  $CuK\alpha$  radiation, in a symmetric geometry (Bragg-Brentano geometry). The obtained diffraction spectra were processed using software developed at the Department of Physical Material Sciences of the National University of Science and Technology (MISiS).

To study the nanostructure of the deposited coatings, a JEM 2100 transmission electron microscope (TEM) (JEOL, Tokyo, Japan) was used at an accelerating voltage of 200 kV. The composition of the coating was studied using a TEM with the INCA Energy Dispersive X-ray (EDX) system (OXFORD Instruments, Oxford, UK).

Hardness and modulus of elasticity were measured using an automatic mechanical tester SV-500 (Nanovea, Irvine, CA, USA) with a nanomodule equipped with a precision piezoelectric drive and a highly sensitive load cell independent of the drive. The measurement method was instrumental indentation using a Berkovich pyramid indenter. The measurements were carried out with a load of 20 mN. Since the hardness of the coatings and the substrate (titanium alloy) differed considerably and the thicknesses of the coatings were small, the hardness measurement proved to be very difficult. Each sample was subjected to 40 measurements with a minimum load (20 mN) to identify the dimensions of the cavity.

The resistance of the coatings to damage during scratch tests was studied on the Nanovea equipment in accordance with ASTM C1624-05, measuring the load from 0 to 40 N.

Electrochemical corrosion studies of Cr-CrN, Ti-TiN, Zr-ZrN, and Mo-MoN coatings were carried out by potentiodynamic polarization measurements (PDP) using an AUTOLAB PGSTAT302 N potentiostat-galvanostat (Metrohm, Herisau, Switzerland) in a standard YaSE-2 three-electrode electrochemical cell with a graphite counter-electrode and a silver/silver chloride-saturated reference electrode at 25 °C. The surface area of the working electrode was 1 cm<sup>2</sup>. All potential values measured against the saturated silver-silver chloride reference electrode were converted to the hydrogen scale. The corrosion resistance of the Cr-CrN, Ti-TiN, Zr-ZrN, and Mo-MoN coatings was estimated using potentiodynamic curves obtained in a 3 wt.% NaCl solution (potential sweep rate  $V_p = 1$  mV/s) at an electrode polarization of  $\pm 800$  mV [83–87], determined by the formula:

$$\eta = E - E_{corr}, \quad (2)$$

where  $E$  is the electrode potential under current and  $E_{corr}$  is the steady-state potential for the corrosion process.

Corrosion currents were calculated using the mathematical modeling functions of the corrosion process in the Nova 2.0 software package using three methods:

1. By the Tafel extrapolation method of the cathode and anode curves with an electrode polarization of  $\pm 100$  mV from the Tafel Equation (3):

$$\eta = a + b \lg i_{corr}, \quad (3)$$

where  $a = \frac{nF}{RT} \lg i_0$  and  $b = \frac{nF}{RT}$  are the Tafel coefficients, with V and V/decade units, respectively,  $i_{corr}$  is the corrosion current density ( $A/cm^2$ ),  $R$  is the universal gas constant,  $8.314 J/(mol \cdot K)$ ,  $T$  is the absolute temperature, K,  $F$  is the Faraday constant,  $96,485.33 C/mol$ ,  $i_0$  is the exchange current density ( $A/cm^2$ ), and  $n$  is the number of electrons involved in the reaction.

2. By the iteration method based on the array of experimental data ( $\eta = \pm 200$  mV) in the Nova 2.0 software package according to Equation (4) [88]:

$$i = i_{corr} \left[ \exp\left(\frac{E - E_{corr}}{b_c}\right) - \exp\left(\frac{E_{corr} - E}{b_a}\right) \right] \quad (4)$$

where  $b_c$  and  $b_a$  are the Tafel coefficients for the anode and cathode process (V/decade).

3. By the method of polarization resistance based on experimental data at low polarizations ( $\eta = \pm 40$  mV):

$$\eta \approx \frac{RT}{nF} \frac{i}{i_0} = R_0 i \quad (5)$$

where  $R_0 = \frac{RT}{i_0 n F}$  is the charge transfer resistance, Ohm [83].

### 3. Results and Discussion

Figure 2 shows a general view of the samples with the considered coatings, showing the typical colors of these coatings.

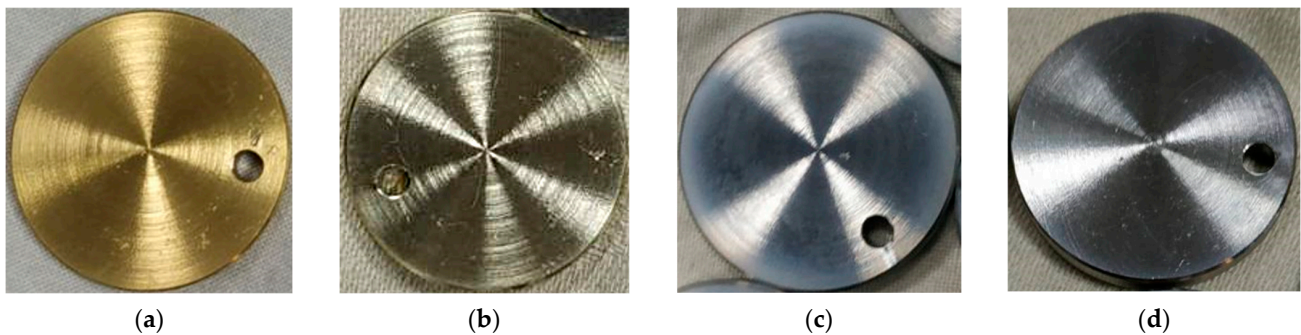


**Figure 2.** Optical microscopy images showing general view of the samples with the (a) Ti-TiN, (b) Zr-ZrN, (c) Cr-CrN, (d) Mo-MoN coatings under consideration.

The surface morphology of the Ti-TiN, Zr-ZrN, Cr-CrN, and Mo-MoN coatings is almost identical, with the surface microparticles being slightly more pronounced in the case of the Ti-TiN and Zr-ZrN coated samples than those coated with Cr-CrN and Mo-MoN (Figure 3). The thickness of the coatings varies from 1.8 to 3.5  $\mu m$ , and they have a columnar grain structure, with clearly pronounced grain boundaries.

The hardness of the prepared coatings and their critical failure load during scratch tests are presented in Table 3. The highest hardness ( $31.7 \pm 1.8$  GPa) was observed for the Zr-ZrN coating, while the lowest ( $20.9 \pm 1.1$  GPa) was for the Mo-MoN coating. During scratch tests, all coatings showed high resistance to damage and strength of adhesive bonds with the substrate, a columnar grain structure, and clearly pronounced grain boundaries.

**Table 3.** Hardness, elastic modulus, and fracture force during the scratch testing of the Ti-TiN, Zr-ZrN, Cr-CrN and Mo-MoN coatings.

Coating	Hardness (GPa)	Elastic Modulus (GPa)	Critical Load $L_{C2}$ (N)
Ti-TiN	$24.9 \pm 1.3$	$266.7 \pm 26.2$	>40
Zr-ZrN	$31.7 \pm 1.8$	$248.5 \pm 37.4$	>40
Cr-CrN	$29.9 \pm 1.3$	$217.2 \pm 28.2$	32
Mo-MoN	$20.9 \pm 1.1$	$226.6 \pm 31.4$	38

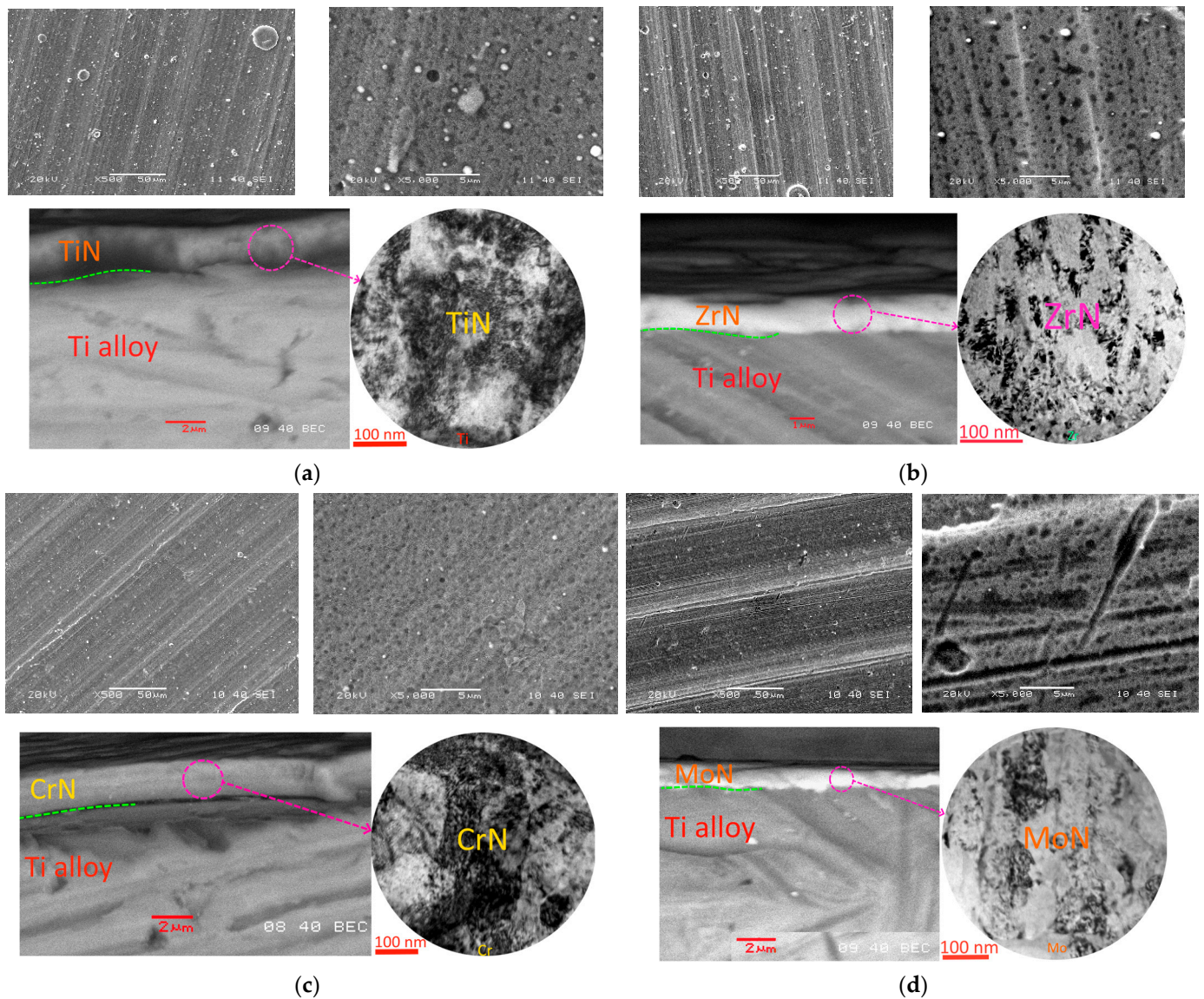


**Figure 3.** Surface morphology (top) and structural features (right—TEM, left—SEM) (bottom) of the samples with the (a) Ti-TiN, (b) Zr-ZrN, (c) Cr-CrN, (d) Mo-MoN coatings.

Phase analysis of the coated samples reveals the presence of a c-TiN, c-ZrN, c-CrN, or c-MoN phase, respectively (Figure 4). On the other hand, the ZrN-coated sample contains an insignificant amount of the  $\alpha$ -Zr phase that may belong to trace amounts of Zr microparticles on the coating surface. The  $\alpha$ -Ti and  $\beta$ -Ti phases of the substrate (titanium alloy) and the intermetallic compound (TiV) were also detected.

The analysis of the evolution of the adhesive component of the friction coefficient  $f_{adh}$  as a function of temperature (Figure 5) shows that with an increase in temperature from 20 to 700 °C, the value of  $f_{adh}$  increases for all samples. With the continuous increase in temperature above 700 °C, different trends appear in the samples with the different coatings. The Mo-MoN-coated sample shows a noticeable decrease in the  $f_{adh}$  value with increasing temperature in the temperature range of 700 to 900 °C. At a temperature of 900 °C, the Mo-MoN-coated sample shows the lowest  $f_{adh}$  value of all considered samples. Such a  $f_{adh}$  behavior for this sample can be associated with the beginning of the formation of a tribologically active molybdenum oxide ( $\text{MoO}_2$ ) film [87]. For the other samples, an increase in the  $f_{adh}$  value is detected up to a temperature of 800 °C, then a slight decrease in temperature is observed from 800 to 900 °C. This decrease can be associated with both

the general plasticization of the material and the beginning of the formation of oxides of the respective metals that affect the tribological properties. At a room temperature of 20 °C, the minimum value of  $f_{adh}$  is detected for the Zr-ZrN coated sample, and the maximum value for the Cr-CrN coated sample, which is in good agreement with the literature results [66–74,87–89]. In the temperature range of 20–400 °C, the sample with the Zr-ZrN coating has the best tribological properties, while at temperatures between 700 and 900 °C, the sample with the Mo-MoN coating provides the minimum  $f_{adh}$  value. All the coatings considered, except for Cr-CrN, lead to a decrease in the  $f_{adh}$  value over the whole temperature range compared to the uncoated sample, as has also been demonstrated for Zr-ZrC coatings [90–92].

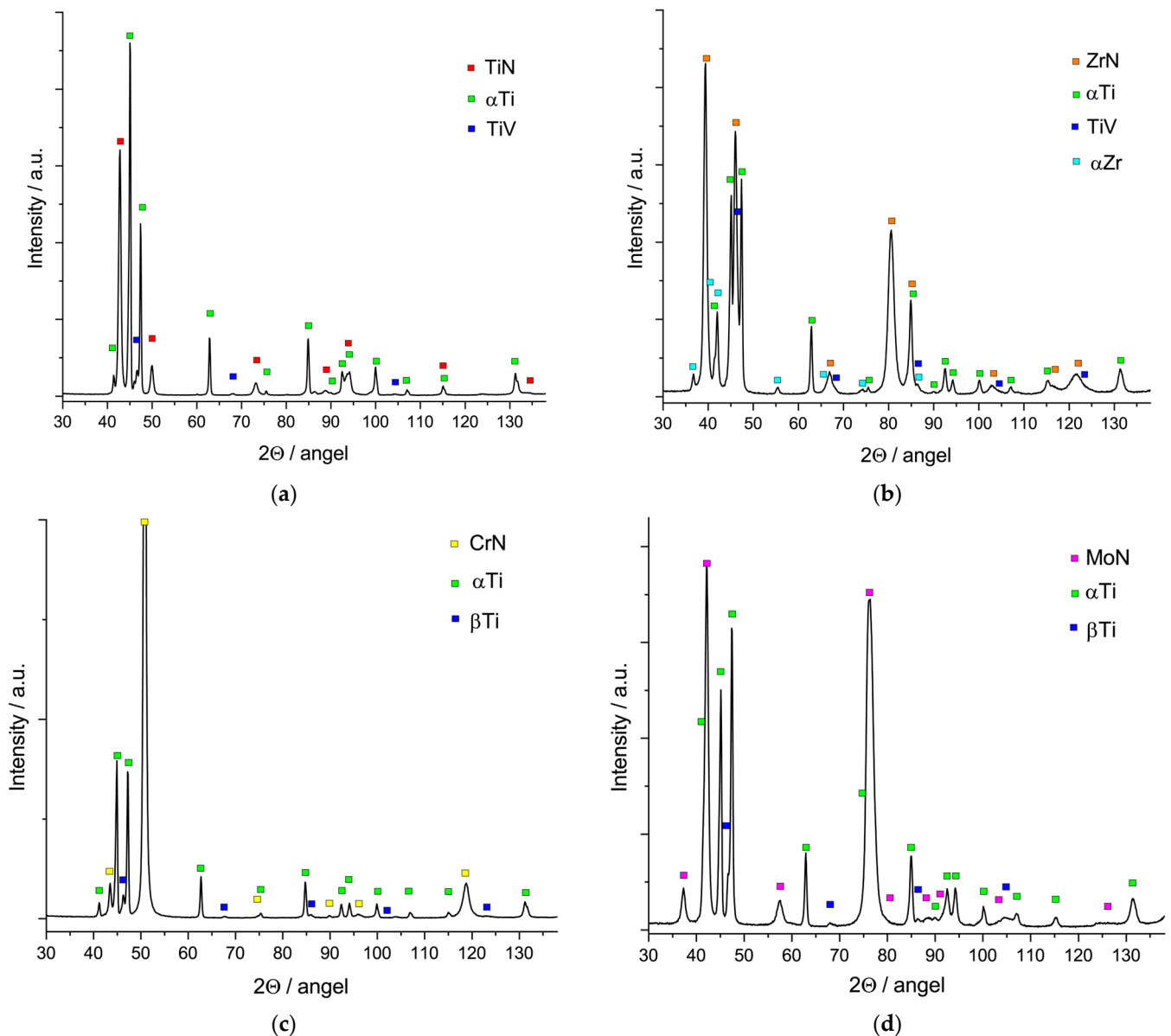


**Figure 4.** Diffraction patterns of the samples with the (a) Ti-TiN, (b) Zr-ZrN, (c) Cr-CrN, and (d) Mo-MoN coatings.

The potentiodynamic polarization curves (the potentiodynamic polarization measurements (PDP)) of the considered Cr-CrN, Ti-TiN, Zr-ZrN, and Mo-MoN coatings on the surface of the Ti-6Al-4V alloy and in the 3 wt.% NaCl solution are shown in Figure 6. The value of the equilibrium (near-equilibrium) potential of the corrosion process for the

uncoated sample of the Ti-6Al-4V alloy is  $-0.045$  V, which indicates the good corrosion resistance of this material in the 3 wt.% NaCl solution in the presence of oxygen and is in good agreement with the results reported in the literature [32,36]. The deposition of the Ti-TiN coating reduces the value of the steady-state corrosion potential to  $-0.078$  V, which is in line with the known corrosion resistance data of Ti-6Al-4V titanium alloy and titanium nitride coating [36,37]. On the other hand, the deposition of Cr-CrN, Zr-ZrN, and Mo-MoN coatings leads to an increase in the equilibrium potential of the corrosion process to  $-0.026$ ,  $-0.017$ , and  $+0.095$  V, respectively, indicating the higher corrosion resistance of the CrN, ZrN, and MoN systems compared to the Ti-6Al-4V alloy and the TiN system.

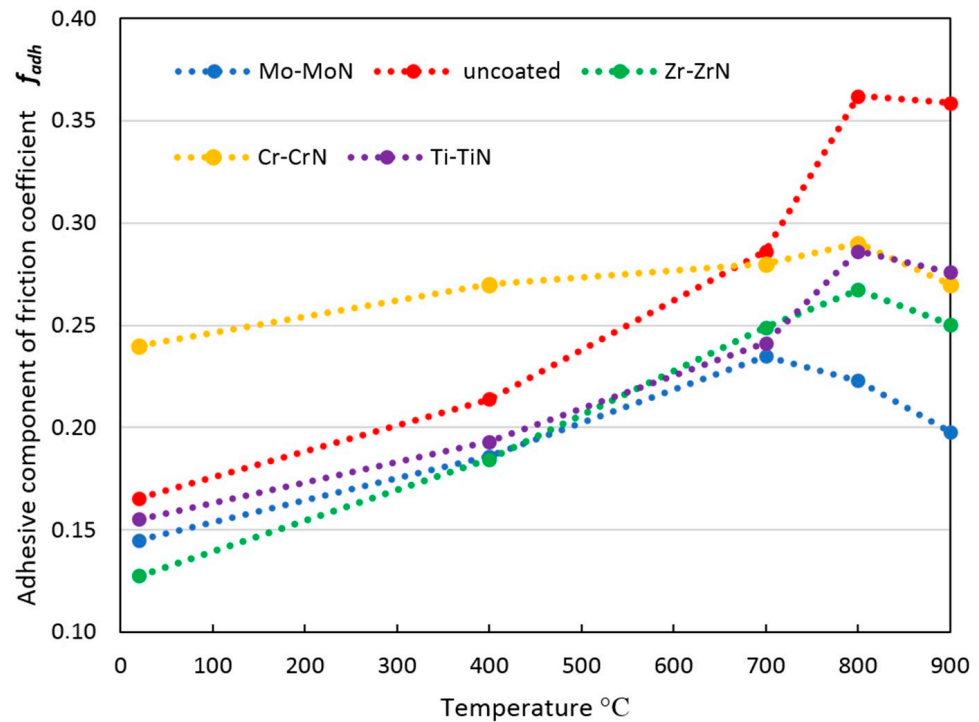


**Figure 5.** Relationship between the adhesive component of friction coefficient  $f_{adh}$  and the temperature for the uncoated samples and the samples with the Ti-TiN, Zr-ZrN, Cr-CrN, Mo-MoN coatings.

To determine the corrosion current density of the studied samples in the 3 wt.% aqueous NaCl solution at the temperature of  $25$  °C, the mathematical modeling of the corrosion process was applied by iterations based on the experimental data and by using Tafel’s extrapolation of the anodic and cathodic polarization curves using the Nova 2.0 software (Table 4 and Figure 7).

**Table 4.** Results of mathematical modeling of the corrosion process on the samples made of Ti-6Al-4V alloy with different coatings in the 3 wt.% aqueous solution of NaCl at the temperature of  $25$  °C, by the method of iterations based on experimental data arrays.

Coating	Corrosion Potential (V)	Corrosion Current Density ( $\mu\text{A}/\text{cm}^2$ )	Corrosion Penetration ( $\mu\text{m}/\text{Year}$ )	Tafel Coef-Ficient $b_c$ (V)	Tafel Coef-Ficient $b_a$ (V)	Calculated Corrosion Potential (V)	Polarization Resistance (kOhm)
Cr-CrN	$-0.026$	0.38	3.4	0.201	0.208	$-0.027$	115.8
Mo-MoN	0.095	8.19	72.2	0.403	0.421	0.098	10.9
Ti-TiN	$-0.078$	1.48	13.0	0.233	2.493	$-0.096$	62.6
Zr-ZrN	$-0.017$	0.34	3.0	0.281	0.367	$-0.021$	202.9
uncoated	$-0.045$	0.69	6.0	0.146	1.201	$-0.062$	82.5

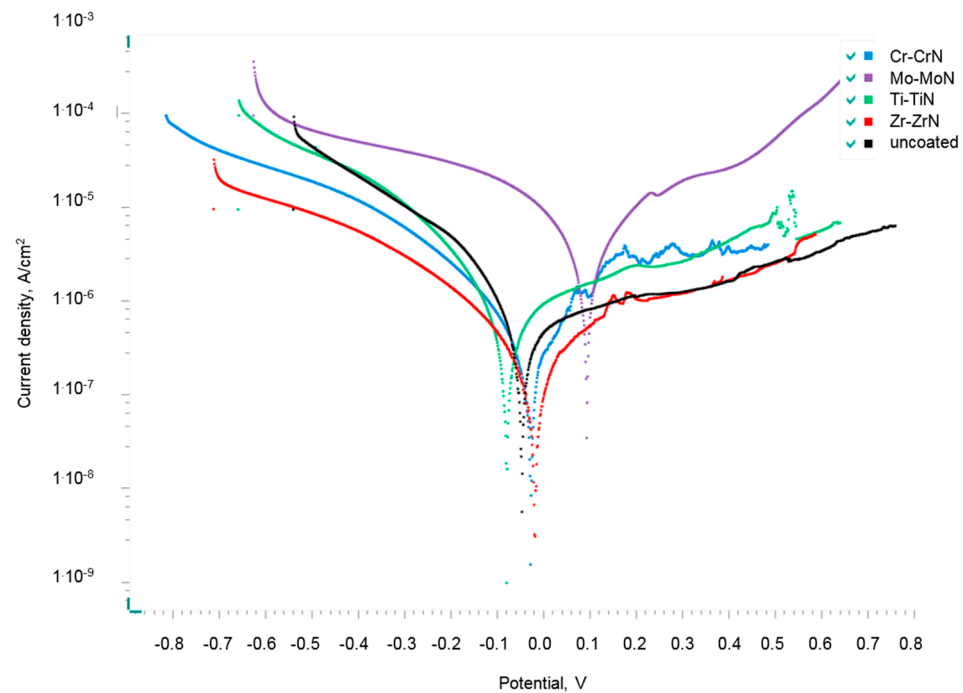


**Figure 6.** Alignment of potentiodynamic curves of the considered coatings of Cr-CrN, Ti-TiN, Zr-ZrN, and Mo-MoN on the substrate of Ti-6Al-4V alloy which were obtained in the 3 wt.% aqueous solution of NaCl (the potential sweep rate  $V_p = 1 \text{ mV/s}$ ).

Figure 7 shows the experimental polarization curves for the Zr-ZrN coated and uncoated Ti-6Al-4V alloy samples, as well as the calculated polarization curves using mathematical modeling by the iteration method according to Equation (3). The experimental and calculated curves coincide completely in the considered potential range. The values of the corrosion current density were calculated considering Equation (3) and using the iteration method in the cathodic and anodic potential range ( $\pm 100 \text{ mV}$ ) of the curves (Figure 7) close to the quasi-equilibrium corrosion potential. The data obtained are presented in Table 5.

**Table 5.** Results of mathematical modeling of the corrosion process on the samples of Ti-6Al-4V alloy with different coatings in the 3 wt.% aqueous solution of NaCl at the temperature of  $25 \text{ }^\circ\text{C}$ , by the method of Tafel extrapolation of the anodic and cathodic polarization curves.

Coating	Corrosion Potential (V)	Corrosion Current Density ( $\mu\text{A}/\text{cm}^2$ )	Corrosion Penetration ( $\mu\text{m}/\text{Year}$ )	Tafel Coef-Ficient $b_c$ (V)	Tafel Coef-Ficient $b_a$ (V)	Calculated Corrosion Potential (V)	Polarization Resistance (kOhm)
Cr-CrN	−0.026	0.218	1.93	0.1552	0.1670	−0.028	29.427
Mo-MoN	0.095	8.190	72.48	0.2055	0.2047	0.098	0.783
Ti-TiN	−0.078	1.480	13.10	0.1268	0.4140	−0.096	4.334
Zr-ZrN	−0.017	0.341	3.02	0.1986	0.2610	−0.021	18.812
uncoated	−0.045	0.390	3.45	0.0969	0.5814	−0.062	16.449

The result of the modeling using the iteration method showed that for all the considered coatings, the value of the coefficient,  $b_c$ , for the cathodic corrosion process is between 0.15 and 0.40 V, which indicates difficulties in the diffusion of the oxidizing agent to reach the surface [86]. On the cathodic branches of the polarization curves in the potential range between  $-0.1$  and  $0.2 \text{ V}$ , the reduction process of dissolved oxygen takes place according to the following reaction:



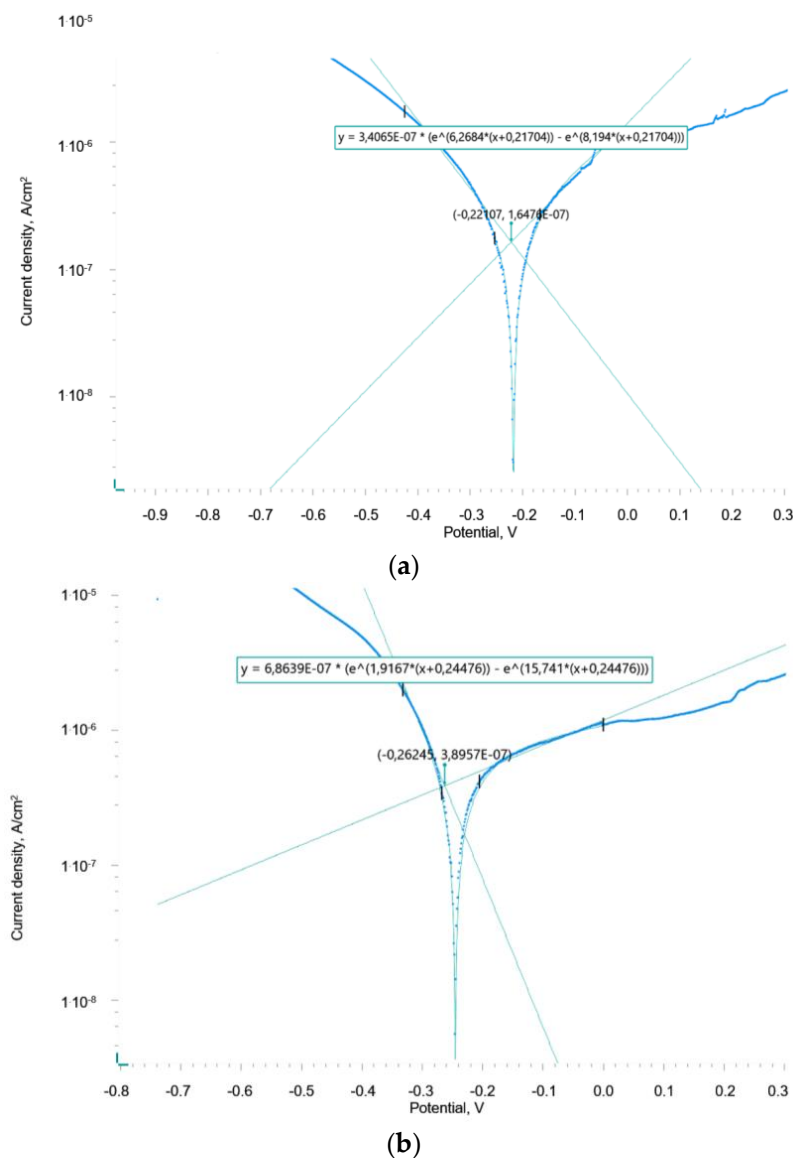


**Figure 7.** Polarization curves of the electrode made of Ti-6Al-4V titanium alloy (a) with the Zr-ZrN coating and (b) without coating in the 3 wt.% solution of NaCl: points—experimental data, straight lines—extrapolation of Tafel sections, curved line—results of mathematical modeling by the iteration method.

Figure 6 shows well-defined linear sections on the anodic part of the curve. The region of cathodic potentials close to the corrosion potential contains information about the cathodic process occurring at the electrode and the anodic dissolution process [84]. The coefficient,  $b_a$ , calculated for the anodic curves according to Equation (4) is between 0.21 and 2.5 V, while from the extrapolation of the Tafel sections, the coefficient,  $b_a$ , for the anodic curves is between 0.17 and 0.58 V, indicating a significant role of diffusion in the corrosion kinetics, which may be due to the formation of oxide and oxonitride films of the respective metals on the surface of Cr-CrN, Ti-TiN, Zr-ZrN, and Mo-MoN coatings as reported in the literature [32,35,38–43,52–55]. The values of the cathode Tafel coefficient ( $b_c$ ) and anode Tafel coefficient ( $b_a$ ) are significantly higher than the same Tafel coefficient with electrochemical kinetics [93].

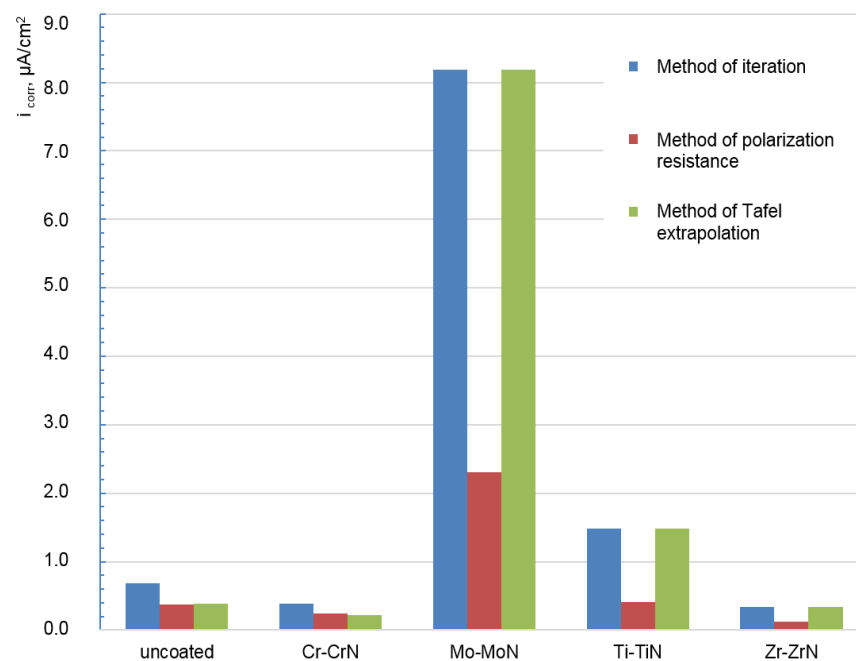
The formation of such dielectric films is accompanied by a sharp increase in the electrical resistance of the coating–electrolyte interface. In this case, Equation (3) and Tafel’s method of extrapolating polarization curves to determine the corrosion rate are obviously of

little use since the corrosion process takes place in the low resistance region [86]. Therefore, a corrosion process was simulated using the polarization resistance method (see Table 6).

**Table 6.** Calculation results of the corrosion process characteristics using the method of determining the polarization resistance in the region of the corrosion potential in the 3 wt.% aqueous solution of NaCl at the temperature of 25 °C.

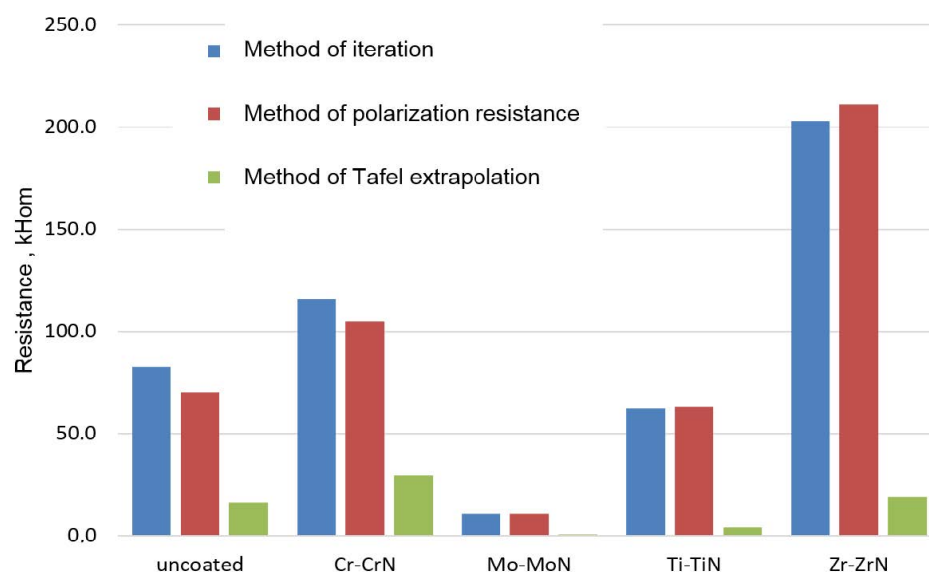
Coating	Corrosion Potential (V)	Corrosion Current Density ( $\mu\text{A}/\text{cm}^2$ )	Corrosion Penetration ( $\mu\text{m}/\text{Year}$ )	Polarization Resistance (kOhm)
Cr-CrN	−0.026	0.248	2.19	105.0
Mo-MoN	0.095	2.310	20.40	11.2
Ti-TiN	−0.078	0.411	3.63	63.3
Zr-ZrN	−0.017	0.123	1.09	210.9
Uncoated	−0.045	0.372	3.28	70.0

Table 6 shows that the current density determined by the polarization resistance method is 3 to 4 times lower than the current density determined by the iteration method according to Equation (3) and by the method of extrapolating the Tafel cross-sections of the anodic and cathodic polarization curves (Figure 8).



**Figure 8.** Comparative diagram of the corrosion current density values for the plates made of Ti-6Al-4V alloy and coated with Cr-CrN, Ti-TiN, Zr-ZrN, and Mo-MoN in the 3 wt.% solution of NaCl, calculated by mathematical modeling of the corrosion process by the methods of iteration, polarization resistance, and Tafel extrapolation.

The comparison of the polarization resistance calculated by the different mathematical models of the corrosion process for the surfaces of Cr-CrN, Ti-TiN, Zr-ZrN, and Mo-MoN coatings in a 3% aqueous NaCl solution at a temperature of 25 °C is shown in Figure 9. The values of the polarization resistance ( $R_o$ ) calculated by the iteration method and the polarization resistance method are almost comparable for all considered samples, while the results of the Tafel extrapolation method give underestimated  $R_o$  values.



**Figure 9.** Comparative diagram of the polarization corrosion resistance values for the plates made of Ti-6Al-4V alloy and coated with Cr-CrN, Ti-TiN, Zr-ZrN, and Mo-MoN coatings in the 3 wt.% solution of NaCl, defined by mathematical modeling of the corrosion process by the iteration methods.

Therefore, it can be concluded that the most appropriate method to evaluate the corrosion process rate for Cr-CrN, Ti-TiN, Zr-ZrN, and Mo-MoN coatings is the polarization resistance calculation method. This is because the corrosion current density is insignificant for these coatings (Figure 8), and it is a linear function of the electrode polarization (Equation (5)) [85]. On the other hand, the iteration method (Equation (4)) is applicable for large electrode polarizations ( $\eta = \pm 200$  mV) at higher current densities [86].

The lowest corrosion currents in the 3 wt.% NaCl solution were obtained for the Zr-ZrN ( $0.123 \mu\text{A}/\text{cm}^2$ ) and Cr-CrN ( $0.248 \mu\text{A}/\text{cm}^2$ ) coatings (Figure 8), which is in good agreement with the literature results [61,94]. Probably, the best corrosion resistance of the ZrN is related to the high value of the contact angle at the solid–liquid interface that was shown in [62].

It should also be noted that the Ti-TiN coating exhibits a corrosion current of  $0.411 \mu\text{A}/\text{cm}^2$ , similar to that of the Ti-6Al-4V alloy (corrosion current of  $0.372 \mu\text{A}/\text{cm}^2$ ) in the 3% NaCl solution, which can be explained by the similarity of the elemental composition of the titanium alloy and the Ti-TiN coating.

The Mo-MoN coating is distinguished by a maximum corrosion current of  $2.310 \mu\text{A}/\text{cm}^2$ , which is most likely associated with the increased oxidative activity of the molybdenum compounds formed during the corrosion process in the 3 wt.% NaCl solution.

#### 4. Conclusions

The mechanical and corrosion resistance properties of Cr-CrN, Ti-TiN, Zr-ZrN, and Mo-MoN two-component nitride coatings deposited on the Ti-6Al-4V alloy substrate were compared, and it was found that:

1. The maximum hardness ( $31.7 \pm 1.8$  GPa) was detected for the Zr-ZrN coating, while the lowest hardness ( $20.9 \pm 1.1$  GPa) was observed for the Mo-MoN coating.
2. The phase analysis reveals the presence of an fcc phase in all coatings: c-TiN, c-ZrN, c-CrN, or c-MoN, respectively.
3. In the temperature range of 20–400 °C, the minimum value of the adhesive component of the friction coefficient  $f_{adh}$  was detected for the sample with the Zr-ZrN coating and in the temperature range of 700–900 °C for the sample with the Mo-MoN coating. Over the whole temperature range, all coatings, except Cr-CrN, lead to a reduction in  $f_{adh}$  compared to the uncoated sample.

4. From the comparison of the corrosion properties of Cr-CrN, Ti-TiN, Zr-ZrN, and Mo-MoN coatings in a 3 wt.% NaCl solution, it was found that the most acceptable method for evaluating the rate of the corrosion process from the analysis of the polarization curves of these coatings is the polarization resistance calculation method. This is due to the formation of dielectric oxide films during the corrosion process of Cr-CrN, Ti-TiN, Zr-ZrN, and Mo-MoN coatings, which is accompanied by a strong increase in the electrical resistance of the coating–electrolyte interface.
5. The minimum corrosion currents in the 3% NaCl solution were observed for the Zr-ZrN ( $0.123 \mu\text{A}/\text{cm}^2$ ) and Cr-CrN ( $0.248 \mu\text{A}/\text{cm}^2$ ) coatings. However, the Mo-MoN coating stands out with an increase in corrosion current ( $2.310 \mu\text{A}/\text{cm}^2$ ) compared to the uncoated Ti-6Al-4V alloy ( $0.372 \mu\text{A}/\text{cm}^2$ ), and this phenomenon is probably due to the oxidative activity of the molybdenum compounds formed during the corrosion process.
6. The Zr-ZrN coating is best suited to improve the tribological and anti-corrosion properties of titanium friction pairs used in media with properties such as those of the 3 wt.% NaCl solution. The improvement of the mechanical and corrosion resistance properties of the materials can be achieved by depositing multi-component coatings based on the ZrN system on their surfaces, as well as by using coatings with nanolayer structures. The properties of these coatings should be investigated further.

**Author Contributions:** Conceptualization, H.T. and A.V.; methodology, A.V. and V.Z.; software, O.S.; validation, H.T., A.V., and V.Z.; formal analysis, V.C.; investigation, H.Y., F.M., C.S., A.S., and V.Z.; resources, A.V.; data curation, A.V. and V.Z.; writing—original draft preparation, H.T., F.M., A.V., and V.Z.; writing—review and editing, V.C., F.M., A.V., and V.Z.; visualization, A.V. and V.Z.; supervision, V.C., A.V.; funding acquisition, H.T. and V.C. All authors have read and agreed to the published version of the manuscript.

**Funding:** This project is funded by the National Natural Science Foundation of China (Grant No. 52275350), Natural Science Foundation of Shanghai (Grant No. 20ZR1422100) and International cooperative scientific research platform of SUES (Grant No. 0301006).

**Institutional Review Board Statement:** Not applicable.

**Informed Consent Statement:** Not applicable.

**Data Availability Statement:** Not applicable.

**Acknowledgments:** The authors would like to express their gratitude to the National University of Science and Technology MISiS for providing the TEM and SEM studies.

**Conflicts of Interest:** The authors declare no conflict of interest.

## References

1. Kaur, M.; Singh, K. Review on titanium and titanium-based alloys as biomaterials for orthopaedical applications. *Mater. Sci. Eng. C* **2019**, *102*, 844–862. [[CrossRef](#)]
2. Zhang, L.-C.; Chen, L.-Y. A Review on Biomedical Titanium Alloys: Recent Progress and Prospect. *Adv. Eng. Mater.* **2019**, *21*, 1801215. [[CrossRef](#)]
3. Zhang, X.; Chen, Y.; Hu, J. Recent advances in the development of aerospace materials. *Prog. Aerosp. Sci.* **2018**, *97*, 22–34. [[CrossRef](#)]
4. Nicholson, J.W. Titanium Alloys for Dental Implants: A Review. *Prosthesis* **2020**, *2*, 100–116. [[CrossRef](#)]
5. Zhang, D.; Sun, S.; Qiu, D.; Gibson, M.A.; Dargusch, M.S.; Brandt, M.; Qian, M.; Easton, M. Metal Alloys for Fusion-Based Additive Manufacturing. *Adv. Eng. Mater.* **2018**, *20*, 1700952. [[CrossRef](#)]
6. Pierce, D.; Haynes, A.; Hughes, J.; Graves, R.; Maziasz, P.; Muralidharan, G.; Shyam, A.; Wang, B.; England, R.; Daniel, C. High temperature materials for heavy duty diesel engines: Historical and future trends. *Prog. Mater. Sci.* **2019**, *103*, 109–179. [[CrossRef](#)]
7. Qiu, G.; Guo, Y. Current situation and development trend of titanium metal industry in China. *Int. J. Miner. Met. Mater.* **2022**, *29*, 599–610. [[CrossRef](#)]
8. Xue, T.; Attarilar, S.; Liu, S.; Liu, J.; Song, X.; Li, L.; Zhao, B.; Tang, Y. Surface modification techniques of titanium and its alloys to functionally optimize their biomedical properties: Thematic review. *Front. Bioeng. Biotechnol.* **2020**, *8*, 603072. [[CrossRef](#)]
9. Berthaud, M.; Popa, I.; Chassagnon, R.; Heintz, O.; Lavková, J.; Chevalier, S. Study of titanium alloy Ti6242S oxidation behaviour in air at 560 °C: Effect of oxygen dissolution on lattice parameters. *Corros. Sci.* **2020**, *164*, 108049. [[CrossRef](#)]

10. Dai, J.; Zhu, J.; Chen, C.; Weng, F. High temperature oxidation behavior and research status of modifications on improving high temperature oxidation resistance of titanium alloys and titanium aluminides: A review. *J. Alloy. Compd.* **2016**, *685*, 784–798. [[CrossRef](#)]
11. Ma, K.; Zhang, R.; Sun, J.; Liu, C. Oxidation Mechanism of Biomedical Titanium Alloy Surface and Experiment. *Int. J. Corros.* **2020**, *2020*, 1678615. [[CrossRef](#)]
12. Chaze, A.M.; Coddet, C. Influence of alloying elements on the dissolution of oxygen in the metallic phase during the oxidation of titanium alloys. *J. Mater. Sci.* **1987**, *22*, 1206–1214. [[CrossRef](#)]
13. Eliaz, N. Corrosion of metallic biomaterials: A review. *Materials* **2019**, *12*, 407. [[CrossRef](#)]
14. Hanawa, T. Titanium-tissue interface reaction and its control with surface treatment. *Front. Bioeng. Biotechnol.* **2019**, *7*, 170. [[CrossRef](#)]
15. Sidhu, S.S.; Singh, H.; Gepreel, M.A.-H. A review on alloy design, biological response, and strengthening of  $\beta$ -titanium alloys as biomaterials. *Mater. Sci. Eng. C* **2021**, *121*, 111661. [[CrossRef](#)] [[PubMed](#)]
16. Chouirfa, H.; Bouloussa, H.; Migonney, V.; Falentin-Daudré, C. Review of titanium surface modification techniques and coatings for antibacterial applications. *Acta Biomater.* **2019**, *83*, 37–54. [[CrossRef](#)] [[PubMed](#)]
17. Zhang, L.-C.; Chen, L.-Y.; Wang, L. Surface Modification of Titanium and Titanium Alloys: Technologies, Developments, and Future Interests. *Adv. Eng. Mater.* **2020**, *22*, 1901258. [[CrossRef](#)]
18. Spriano, S.; Yamaguchi, S.; Baino, F.; Ferraris, S. A critical review of multifunctional titanium surfaces: New frontiers for improving osseointegration and host response, avoiding bacteria contamination. *Acta Biomater.* **2018**, *79*, 1–22. [[CrossRef](#)] [[PubMed](#)]
19. Grigoriev, S.; Vereschaka, A.; Milovich, F.; Andreev, N.; Bublikov, J.; Sitnikov, N.; Sotova, C.; Kutina, N. Investigation of wear mechanisms of multilayer nanostructured wear-resistant coatings during turning of steel. Part 2: Diffusion, oxidation processes and cracking in Ti-TiN-(Ti,Cr,Mo,Al)N coating. *Wear* **2021**, *486–487*, 204096. [[CrossRef](#)]
20. Vereschaka, A.; Tabakov, V.; Grigoriev, S.; Sitnikov, N.; Oganyan, G.; Andreev, N.; Milovich, F. Investigation of wear dynamics for cutting tools with multilayer composite nanostructured coatings in turning constructional steel. *Wear* **2019**, *420–421*, 17–37. [[CrossRef](#)]
21. Stein, T.; Ein-Eli, Y. Proton exchange membrane (PEM) fuel cell bipolar plates prepared from a physical vapor deposition (PVD) titanium nitride (TiN) coated AISI416 stainless-steel. *SN Appl. Sci.* **2019**, *1*, 14–20. [[CrossRef](#)]
22. Asri, N.F.; Husaini, T.; Sulong, A.B.; Majlan, E.H.; Daud, W.R.W. Coating of stainless steel and titanium bipolar plates for anticorrosion in PEMFC: A review. *Int. J. Hydrog. Energy* **2017**, *42*, 9135–9148. [[CrossRef](#)]
23. Antunes, R.A.; Oliveira, M.C.L.; Ett, G.; Ett, V. Corrosion of metal bipolar plates for PEM fuel cells: A review. *Int. J. Hydrogen Energy* **2010**, *35*, 3632–3647. [[CrossRef](#)]
24. Ho, W.Y.; Pan, H.J.; Chang, C.L.; Wang, D.Y.; Hwang, J.J. Corrosion and electrical properties of multi-layered coatings on stainless steel for PEMFC bipolar plate applications. *Surf. Coat. Technol.* **2007**, *202*, 1297–1301. [[CrossRef](#)]
25. Kahraman, H.; Cevik, I.; Dündar, F.; Ficici, F. The corrosion resistance behaviors of metallic bipolar plates for PEMFC coated with physical vapor deposition (PVD): An experimental study. *Arab. J. Sci. Eng.* **2016**, *41*, 1961–1968. [[CrossRef](#)]
26. Wang, Y.; Northwood, D.O. Effect of substrate material on the corrosion of TiN-coated stainless steels in simulated anode and cathode environments of proton exchange membrane fuel cells. *J. Power Sources* **2009**, *191*, 483–488. [[CrossRef](#)]
27. Wang, H.; Turner, J.A. Ferritic stainless steels as bipolar plate material for polymer electrolyte membrane fuel cells. *J. Power Sources* **2004**, *128*, 193–200. [[CrossRef](#)]
28. Zhang, D.; Duan, L.; Guo, L.; Wang, Z.; Zhao, J.; Tuan, W.H.; Niihara, K. TiN-coated titanium as the bipolar plate for PEMFC by multi-arc ion plating. *Int. J. Hydrogen Energy* **2011**, *36*, 9155–9161. [[CrossRef](#)]
29. Ren, Z.; Zhang, D.; Wang, Z. Stacks with TiN/titanium as the bipolar plate for PEMFCs. *Energy* **2012**, *48*, 577–581. [[CrossRef](#)]
30. Wang, H.; Turner, J.A. Reviewing metallic PEMFC bipolar plates. *Fuel Cells* **2010**, *10*, 510–519. [[CrossRef](#)]
31. Li, R.; Wang, S.; Pu, J.; Zhou, D.; Yu, M.; Wei, Y.; Guo, W. Study of NaCl-induced hot-corrosion behavior of TiN single-layer and TiN/Ti multilayer coatings at 500 °C. *Corros. Sci.* **2021**, *192*, 109838. [[CrossRef](#)]
32. Li, R.; Wang, S.; Zhou, D.; Pu, J.; Yu, M.; Guo, W. A new insight into the NaCl-induced hot corrosion mechanism of TiN coatings at 500 °C. *Corros. Sci.* **2020**, *174*, 108794. [[CrossRef](#)]
33. Vega, J.; Scheerer, H.; Andersohn, G.; Oechsner, M. Experimental studies of the effect of Ti interlayers on the corrosion resistance of TiN PVD coatings by using electrochemical methods. *Corros. Sci.* **2018**, *133*, 240–250. [[CrossRef](#)]
34. Zhou, D.P.; Peng, H.; Zhu, L.; Guo, H.B.; Gong, S.K. Microstructure, hardness and corrosion behaviour of TiN/Ti multilayer coatings produced by plasma activated EB-PVD. *Surf. Coat. Technol.* **2014**, *258*, 102–107. [[CrossRef](#)]
35. Shukla, K.; Rane, R.; Alphonsa, J.; Maity, P.; Mukherjee, S. Structural, mechanical and corrosion resistance properties of Ti/TiN bilayers deposited by magnetron sputtering on AISI 316L. *Surf. Coat. Technol.* **2017**, *324*, 167–174. [[CrossRef](#)]
36. Zhang, M.M.; Xin, L.; Ding, X.Y.; Zhu, S.L.; Wang, F.H. Effects Ti/TiAlN composite multilayer coatings on corrosion resistance of titanium alloy in solid NaCl-H<sub>2</sub>O-O<sub>2</sub> at 600 °C. *J. Alloy. Compd.* **2017**, *734*, 307–317. [[CrossRef](#)]
37. Zhang, M.; Niu, Y.; Xin, L.; Su, J.; Li, Y.; Wu, T.; Zhao, H.; Zhang, Y.; Xie, W.; Zhu, S.; et al. Studies on corrosion resistance of thick Ti/TiN multilayer coatings under solid NaCl-H<sub>2</sub>O-O<sub>2</sub> at 450 °C. *Ceram. Int.* **2020**, *46*, 19274–19284. [[CrossRef](#)]
38. Li, R.; Cai, Y.; Wippermann, K.; Lehnert, W. Bilayer CrN/Cr coating-modified 316L stainless steel bipolar plates for high temperature polymer electrolyte fuel cells. *J. Power Sources* **2019**, *434*, 226718. [[CrossRef](#)]

39. Barranco, J.; Barreras, F.; Lozano, A.; Maza, M. Influence of CrN-coating thickness on the corrosion resistance behaviour of aluminium-based bipolar plates. *J. Power Sources* **2011**, *196*, 4283–4289. [[CrossRef](#)]
40. Hu, Y.Q.; Chen, F.; Xiang, Z.D. Cr<sub>2</sub>N coated martensitic stainless steels by pack cementation process as materials for bipolar plates of proton exchange membrane fuel cells. *J. Power Sources* **2019**, *414*, 167–173. [[CrossRef](#)]
41. Guan, X.Y.; Wang, Y.X.; Zhang, G.G.; Jiang, X.; Wang, L.P.; Xue, Q.J. Microstructures and properties of Zr/CrN multilayer coatings fabricated by multi-arc ion plating. *Tribol. Int.* **2017**, *106*, 78–87. [[CrossRef](#)]
42. Cai, F.; Yang, Q.; Huang, X.; Wei, R. Microstructure, and corrosion behavior of CrN and CrSiCN coatings. *J. Mater. Eng. Perform.* **2010**, *19*, 721–727. [[CrossRef](#)]
43. Chun, S.-Y. The structure and properties of inductively coupled plasma assisted magnetron sputtered nanocrystalline CrN coatings in corrosion protective die casting molds. *J. Nanosci. Nanotechnol.* **2015**, *15*, 5354–5357. [[CrossRef](#)] [[PubMed](#)]
44. Li, Z.; Liu, C.; Chen, Q.; Yang, J.; Liu, J.; Yang, H.; Zhang, W.; Zhang, R.; He, L.; Long, J.; et al. Microstructure, high-temperature corrosion and steam oxidation properties of Cr/CrN multilayer coatings prepared by magnetron sputtering. *Corros. Sci.* **2021**, *191*, 109755. [[CrossRef](#)]
45. Meng, C.; Yang, L.; Wu, Y.; Tan, J.; Dang, W.; He, X.; Ma, X. Study of the oxidation behavior of CrN coating on Zr alloy in air. *J. Nucl. Mater.* **2019**, *515*, 354–369. [[CrossRef](#)]
46. Lin, J.; Zhang, N.; Sproul, W.D.; Moore, J.J. A comparison of the oxidation behavior of CrN films deposited using continuous dc, pulsed dc and modulated pulsed power magnetron sputtering. *Surf. Coat. Technol.* **2012**, *206*, 3283–3290. [[CrossRef](#)]
47. Liu, C.; Leyland, A.; Bi, Q.; Matthews, A. Corrosion resistance of multi-layered plasma-assisted physical vapour deposition TiN and CrN coatings. *Surf. Coat. Technol.* **2001**, *141*, 164–173. [[CrossRef](#)]
48. Liu, C.; Bi, Q.; Leyland, A.; Matthews, A. An electrochemical impedance spectroscopy study of the corrosion behaviour of PVD coated steels in 0.5 N NaCl aqueous solution: Part I. Establishment of equivalent circuits for EIS data modelling. *Corros. Sci.* **2003**, *45*, 1243–1256. [[CrossRef](#)]
49. Gilewicz, A.; Chmielewska, P.; Murzynski, D.; Dobruchowska, E.; Warcholinski, B. Corrosion resistance of CrN and CrCN/CrN coatings deposited using cathodic arc evaporation in Ringer's and Hank's solutions. *Surf. Coat. Technol.* **2016**, *299*, 7–14. [[CrossRef](#)]
50. Close, T.F.; Lia, T.M.; Liu, H.M.; Wei, S.H.; Hussaina, J.X.; Wang, W.; Zeng, X.H.; Peng, Z.C. Wang. First-principles calculations of the twin boundary energies and adhesion energies of interfaces for cubic face-centered transition-metal nitrides and carbides. *Appl. Surf. Sci.* **2015**, *355*, 1132–1135.
51. Roman, D.; Bernardi, J.; de Amorim, C.L.; de Souza, F.S.; Spinelli, A.; Giacomelli, C.; Figueroa, C.A.; Baumvol, I.J.; Basso, R.L. Effect of deposition temperature on microstructure and corrosion resistance of ZrN thin films deposited by DC reactive magnetron sputtering. *Mater. Chem. Phys.* **2011**, *130*, 147–153. [[CrossRef](#)]
52. Zhang, S.; Wang, J.; Wu, R.; Liu, L.; Pan, B.; Liu, C. Structural and corrosion resistance properties of sputtered zirconium nitride thin films as electrode material for supercapacitor. *J. Alloy. Compd.* **2022**, *900*, 163506. [[CrossRef](#)]
53. Jin, W.; Zhou, H.; Li, J.; Ruan, Q.; Li, J.; Peng, X.; Li, W.; Chu, P.K. Zirconium-based nanostructured coating on the Mg-4Y-3Re alloy for corrosion retardation. *Chem. Phys. Lett.* **2020**, *756*, 137824. [[CrossRef](#)]
54. Sarioglu, C.; Demirler, U.; Kazmanli, M.K.; Urgen, M. Measurement of residual stresses by X-ray diffraction techniques in MoN and Mo<sub>2</sub>N coatings deposited by arc PVD on high-speed steel substrate. *Surf. Coat. Technol.* **2005**, *190*, 238–243. [[CrossRef](#)]
55. Lunarska, E. Corrosion resistance of TiN and MoN coated grey cast iron in acid solutions. *Mater. Corros. Werkst. Und Korrosion.* **1997**, *48*, 101–109. [[CrossRef](#)]
56. Lee, S.H.; Kakati, N.; Maiti, J.; Jee, S.H.; Kalita, D.J.; Yoon, Y.S. Corrosion and electrical properties of CrN- and TiN-coated 316L stainless steel used as bipolar plates for polymer electrolyte membrane fuel cells. *Thin Solid Film.* **2013**, *529*, 374–379. [[CrossRef](#)]
57. Suo, X.; Guo, C.; Kong, D.; Wang, L. Corrosion behaviour of TiN and CrN coatings produced by magnetron sputtering process on aluminium alloy. *Int. J. Electrochem. Sci.* **2019**, *14*, 826–837. [[CrossRef](#)]
58. Nam, N.D.; Kim, M.J.; Jo, D.S.; Kim, J.G.; Yoon, D.H. Corrosion protection of Ti/TiN, Cr/TiN, Ti/CrN, and Cr/CrN multi-coatings in simulated proton exchange membrane fuel cell environment. *Thin Solid Film.* **2013**, *545*, 380–384. [[CrossRef](#)]
59. Chim, Y.C.; Ding, X.Z.; Zeng, X.T.; Zhang, S. Oxidation resistance of TiN, CrN, TiAlN and CrAlN coatings deposited by lateral rotating cathode arc. *Thin Solid Film.* **2009**, *517*, 4845–4849. [[CrossRef](#)]
60. Ma, Z.-K.; Gao, Y.; Cai, H.-W.; Wang, C.; Yuan, L.; Zhang, Y.; Wu, W.-Q. Corrosion resistance of TiN and CrN coatings with arc ion plating on 201 stainless steel surfaces. *Corros. Prot.* **2013**, *34*, 670–672.
61. Yi, P.; Zhu, L.; Dong, C.; Xiao, K. Corrosion and interfacial contact resistance of 316L stainless steel coated with magnetron sputtered ZrN and TiN in the simulated cathodic environment of a proton-exchange membrane fuel cell. *Surf. Coat. Technol.* **2019**, *363*, 198–202. [[CrossRef](#)]
62. Blanco, D.; Viesca, J.L.; Mallada, M.T.; Ramajo, B.; González, R.; Battez, A.H. Wettability and corrosion of [NTf<sub>2</sub>] anion-based ionic liquids on steel and PVD (TiN, CrN, ZrN) coatings. *Surf. Coat. Technol.* **2016**, *302*, 13–21. [[CrossRef](#)]
63. Samim, P.M.; Fattah-Alhosseini, A.; Elmkhah, H.; Imantalab, O. A study on the corrosion resistance of ZrN/CrN multilayer nanostructured coating applied on AISI 304 stainless steel using Arc-PVD method in 3.5 wt% NaCl solution. *Mater. Res. Express* **2019**, *6*, 126426. [[CrossRef](#)]
64. Zhang, M.; Kim, K.H.; Shao, Z.; Wang, F.; Zhao, S.; Suo, N. Effects of Mo content on microstructure and corrosion resistance of arc ion plated Ti-Mo-N films on 316L stainless steel as bipolar plates for polymer exchange membrane fuel cells. *J. Power Sources* **2014**, *253*, 201–204. [[CrossRef](#)]

65. Jin, J.; Liu, H.; Zheng, D.; Zhu, Z. Effects of Mo content on the interfacial contact resistance and corrosion properties of CrN coatings on SS316L as bipolar plates in simulated PEMFCs environment. *Int. J. Hydrogen Energy* **2018**, *43*, 10048–10060. [[CrossRef](#)]
66. Grigoriev, S.; Vereschaka, A.; Milovich, F.; Sitnikov, N.; Andreev, N.; Bublikov, J.; Kutina, N. Investigation of the properties of the Cr,Mo-(Cr,Mo,Zr,Nb)N-(Cr,Mo,Zr,Nb,Al)N multilayer composite multicomponent coating with nanostructured wear-resistant layer. *Wear* **2021**, *468–469*, 203597. [[CrossRef](#)]
67. Grigoriev, S.; Vereschaka, A.; Milovich, F.; Tabakov, V.; Sitnikov, N.; Andreev, N.; Sviridova, T.; Bublikov, J. Investigation of multicomponent nanolayer coatings based on nitrides of Cr, Mo, Zr, Nb, and Al. *Surf. Coat. Technol.* **2020**, *401*, 126258. [[CrossRef](#)]
68. Vereschaka, A.; Tabakov, V.; Grigoriev, S.; Sitnikov, N.; Milovich, F.; Andreev, N.; Sotova, C.; Kutina, N. Investigation of the influence of the thickness of nanolayers in wear-resistant layers of Ti-TiN-(Ti,Cr,Al)N coating on destruction in the cutting and wear of carbide cutting tools. *Surf. Coat. Technol.* **2020**, *385*, 125402. [[CrossRef](#)]
69. Vereschaka, A.A.; Bublikov, J.I.; Sitnikov, N.N.; Oganyan, G.V.; Sotova, C.S. Influence of nanolayer thickness on the performance properties of multilayer composite nano-structured modified coatings for metal-cutting tools. *Int. J. Adv. Manuf. Technol.* **2018**, *95*, 2625–2640. [[CrossRef](#)]
70. Vereschaka, A.; Tabakov, V.; Grigoriev, S.; Sitnikov, N.; Milovich, F.; Andreev, N.; Bublikov, J. Investigation of wear mechanisms for the rake face of a cutting tool with a multilayer composite nanostructured Cr-CrN-(Ti,Cr,Al,Si)N coating in high-speed steel turning. *Wear* **2019**, *438–439*, 203069. [[CrossRef](#)]
71. Vereschaka, A.; Tabakov, V.; Grigoriev, S.; Sitnikov, N.; Andreev, N.; Milovich, F. Investigation of wear and diffusion processes on rake faces of carbide inserts with Ti-TiN-(Ti,Al,Si)N composite nanostructured coating. *Wear* **2018**, *416–417*, 72–80. [[CrossRef](#)]
72. Vereschaka, A.A.; Vereschaka, A.S.; Grigoriev, S.N.; Kirillov, A.K.; Khaustova, O.U. Development and research of environmentally friendly dry technological machining system with compensation of physical function of cutting fluids. *Procedia CIRP* **2013**, *7*, 311–316. [[CrossRef](#)]
73. Grigoriev, S.; Vereschaka, A.; Uglov, V.; Milovich, F.; Cherenda, N.; Andreev, N.; Migranov, M.; Seleznev, A. Influence of tribological properties of Zr-ZrN-(Zr,Cr,Al)N and Zr-ZrN-(Zr,Mo,Al)N multilayer nanostructured coatings on the cutting properties of coated tools during dry turning of Inconel 718 alloy. *Wear* **2023**, *512–513*, 204521. [[CrossRef](#)]
74. Grigoriev, S.; Vereschaka, A.; Milovich, F.; Andreev, N.; Bublikov, J.; Seleznev, A.; Kutina, N. Influence of Mo content on the properties of multilayer nanostructured coatings based on the (Mo,Cr,Al)N system. *Tribol. Int.* **2022**, *174*, 107741. [[CrossRef](#)]
75. Vereschaka, A.; Milovich, F.; Andreev, N.; Sotova, C.; Alexandrov, I.; Muranov, A.; Mikhailov, M.; Tatarkanov, A. Investigation of the structure and phase composition of the microdroplets formed during the deposition of PVD coatings. *Surf. Coat. Technol.* **2022**, *441*, 128574. [[CrossRef](#)]
76. Grigoriev, S.; Vereschaka, A.; Zelenkov, V.; Sitnikov, N.; Bublikov, J.; Milovich, F.; Andreev, N.; Mustafaev, E. Specific features of the structure and properties of arc-PVD coatings depending on the spatial arrangement of the sample in the chamber. *Vacuum* **2022**, *200*, 111047. [[CrossRef](#)]
77. Grigoriev, S.; Vereschaka, A.; Zelenkov, V.; Sitnikov, N.; Bublikov, J.; Milovich, F.; Andreev, N.; Sotova, C. Investigation of the influence of the features of the deposition process on the structural features of microparticles in PVD coatings. *Vacuum* **2022**, *202*, 111144. [[CrossRef](#)]
78. Shuster, L.S. *Adhesive Interaction of the Cutting Tool with the Material Being Processed*; Mashinostroeniye: Moscow, Russia, 1988; p. 96.
79. Vereschaka, A.; Grigoriev, S.; Tabakov, V.; Migranov, M.; Sitnikov, N.; Milovich, F.; Andreev, N. Influence of the nanostructure of Ti-TiN-(Ti,Al,Cr)N multilayer composite coating on tribological properties and cutting tool life. *Tribol. Int.* **2020**, *150*, 106388. [[CrossRef](#)]
80. Grigoriev, S.; Vereschaka, A.; Milovich, F.; Migranov, M.; Andreev, N.; Bublikov, J.; Sitnikov, N.; Oganyan, G. Investigation of the tribological properties of Ti-TiN-(Ti, Al, Nb, Zr)N composite coating and its efficiency in increasing wear resistance of metal cutting tools. *Tribol. Int.* **2021**, *164*, 107236. [[CrossRef](#)]
81. Vereschaka, A.; Milovich, F.; Migranov, M.; Andreev, N.; Alexandrov, I.; Muranov, A.; Mikhailov, M.; Tatarkanov, A. Investigation of the tribological and operational properties of  $(Me_x, Mo_y, Al_{1-(x+y)})N$  (Me—Ti, Zr or Cr) coatings. *Tribol. Int.* **2022**, *165*, 107305. [[CrossRef](#)]
82. Vereschaka, A.; Grigoriev, S.; Milovich, F.; Sitnikov, N.; Migranov, M.; Andreev, N.; Bublikov, J.; Sotova, C. Investigation of tribological and functional properties of Cr, Mo-(Cr, Mo)N-(Cr, Mo, Al)N multilayer composite coating. *Tribol. Int.* **2021**, *155*, 106804. [[CrossRef](#)]
83. Poorqasemi, E.; Abootalebi, O.; Peikari, M.; Haqdar, F. Investigating accuracy of the Tafel extrapolation method in HCl solutions. *Corros. Sci.* **2009**, *51*, 1043–1054. [[CrossRef](#)]
84. Mansfeld, F.; Fontana, G.; Staehle, R.W. The Polarization Resistance Technique for Measuring Corrosion Currents. *Adv. Corros. Sci. Technol.* **1976**, *6*, 163–175.
85. Rybalka, K.V.; Beketaeva, L.A.; Davydov, A.D. Estimation of corrosion current by the analysis of polarization curves: Electrochemical kinetics mode. *Russ. J. Electrochem.* **2014**, *50*, 108. [[CrossRef](#)]
86. Sinkeviciute, D.; Baltrusaitis, J.; Dukstiene, N. Layered molybdenum oxide thin films electrodeposited from sodium citrate electrolyte solution. *J. Solid-State Electrochem.* **2011**, *15*, 711–723. [[CrossRef](#)]
87. de Castro, I.A.; Datta, R.S.; Ou, J.Z.; Castellanos-Gomez, A.; Sriram, S.; Daeneke, T.; Kalantar Zadeh, K. Molybdenum Oxides—From Fundamentals to Functionality. *Adv. Mater.* **2017**, *29*, 1701619. [[CrossRef](#)]

88. Chayeuski, V.; Taleb, A.; Zhylinski, V.; Kuleshov, A.; Shtempliuk, R. Preparation and Characterization of the Cr-Nanodiamonds/MoN Coatings with Performant Mechanical Properties. *Coatings* **2022**, *12*, 1012. [[CrossRef](#)]
89. Chayeuski, V.; Zhylinski, V.; Grishkevich, A.; Rudak, P.; Barcik, S. Influence of high energy treatment on wear of edges knives of wood-cutting tools. *MM Sci. J.* **2016**, *12*, 1519–1523. [[CrossRef](#)]
90. Chayeuski, V.; Zhylinski, V.; Cernashejus, O.; Visniakov, N.; Mikalauskas, G. Structural and Mechanical Properties of the ZrC/Ni-Nanodiamond Coating Synthesized by the PVD and Electroplating Processes for the Cutting Knives. *J. Mater. Eng. Perform.* **2019**, *28*, 1278–1285. [[CrossRef](#)]
91. Zhylinski, V.; Chayeuski, V.; Kuleshov, A.; Koleda, P.; Barcik, S. Investigation of adhesion and wear of ZrC coating on woodcutting tools. *Acta Fac. Tech.* **2019**, *XXIV*, 53–59.
92. Chayeuski, V.V.; Zhylinski, V.V.; Rudak, P.V.; Rusalsky, D.P.; Višniakov, N.; Cernašėjus, O. Characteristics of ZrC/Ni-UDD coatings for a tungsten carbide cutting tool. *Appl. Surf. Sci.* **2018**, *446*, 18–26. [[CrossRef](#)]
93. Thakur, A.; Kaya, S.; Abousalem, A.S.; Kumar, A. Experimental, DFT and MC simulation analysis of Vicia Sativa weed aerial extract as sustainable and eco-benign corrosion inhibitor for mild steel in acidic environment. *Sustain. Chem. Pharm.* **2022**, *29*, 100785. [[CrossRef](#)]
94. Thakur, A.; Kumar, A.; Kaya, S.; Marzouki, R.; Zhang, F.; Guo, L. Recent Advancements in Surface Modification, Characterization and Functionalization for Enhancing the Biocompatibility and Corrosion Resistance of Biomedical Implants. *Coatings* **2022**, *12*, 1459. [[CrossRef](#)]

**Disclaimer/Publisher’s Note:** The statements, opinions and data contained in all publications are solely those of the individual author(s) and contributor(s) and not of MDPI and/or the editor(s). MDPI and/or the editor(s) disclaim responsibility for any injury to people or property resulting from any ideas, methods, instructions or products referred to in the content.